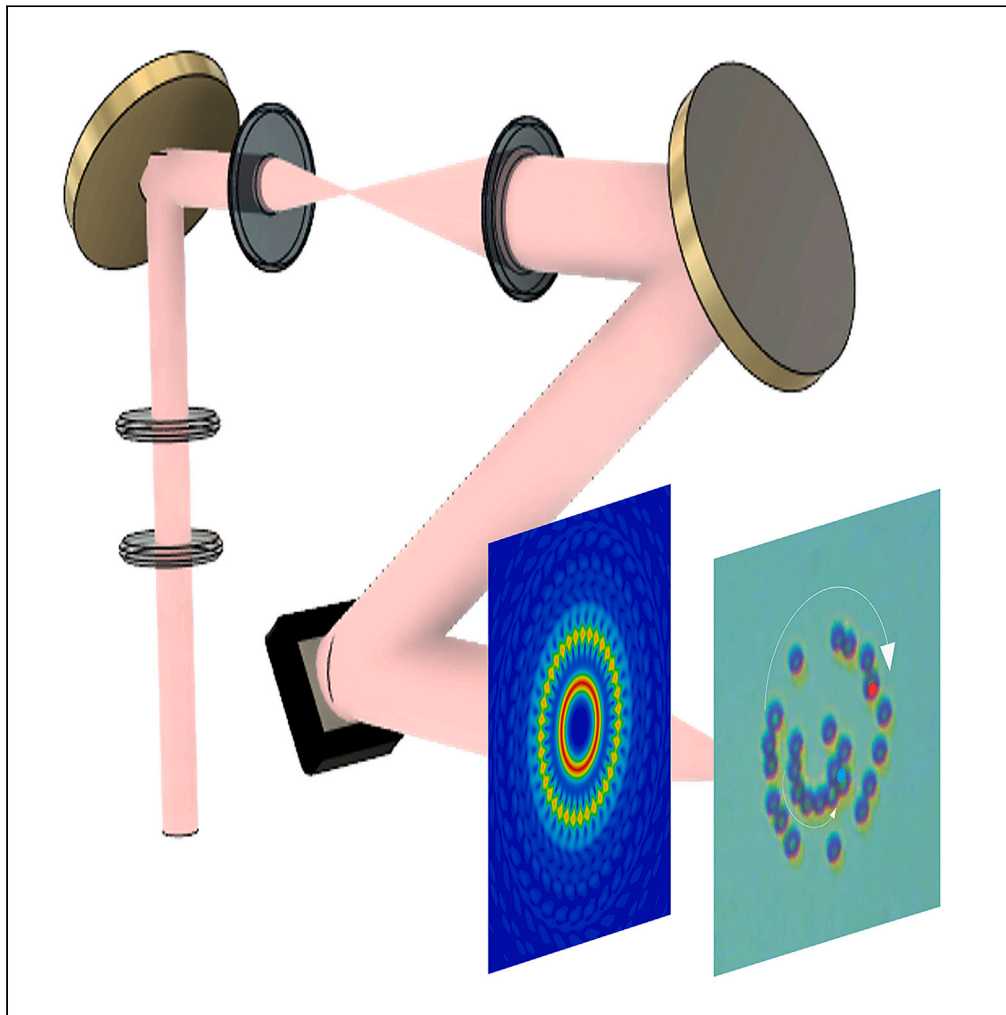**Article**

Multiplexed vortex beam-based optical tweezers generated with spiral phase mask

Francisco M. Muñoz-Pérez, Vicente Ferrando, Walter D. Furlan, Juan C. Castro-Palacio, J. Ricardo Arias-Gonzalez, Juan A. Monsoriu

fmmuope1@upvnet.upv.es

Highlights

Design and implementation of a multiplexed spiral phase mask

Implementation of multiplexed vortex beam-based optical tweezers

Generation of concentric vortex beams with independent topological charges

The transfer of angular momentum to trapped microparticles within each vortex

Article

Multiplexed vortex beam-based optical tweezers generated with spiral phase mask

Francisco M. Muñoz-Pérez,[1,2,4,*] Vicente Ferrando,[1] Walter D. Furlan,[3] Juan C. Castro-Palacio,[1] J. Ricardo Arias-Gonzalez,[1] and Juan A. Monsoriu[1]

SUMMARY

The design and implementation of a multiplexed spiral phase mask in an experimental optical tweezers setup are presented. This diffractive optical element allows the generation of multiple concentric vortex beams with independent topological charges and without amplitude modulation. The generalization of the phase mask for multiple concentric vortices is also shown. The design for a phase mask of two multiplexed vortices with different topological charges is developed. We experimentally show the transfer of angular momentum to the optically trapped microparticles by enabling nearly independent orbiting dynamics around the optical axis within each vortex. The angular velocity of the confined particles versus the optical power in the focal region is also discussed for different combinations of topological charges.

INTRODUCTION

Vortex dynamics is present in diverse scientific areas, such as gravitation[1] or fluidics.[2] In optics, since the first proposal of an optical vortex in the late 1980s,[3] multiple applications have been developed for trapping and manipulation, communications, encryption and biosciences, among others.[4–11] In 1996, Gargaran et al. showed the stable trapping of low refractive index microparticles through optical vortices.[12] With the development of new photonic technologies and components, the implementation of new strategies in vortex beam generation has grown, most notably with spiral phase plates.[13,14] Previous works have shown that spiral phase zone plates, also known as vortex lenses, allow the generation of a series of optical vortices distributed along the optical axis.[9,15] These vortex lenses are diffractive optical elements (DOEs) that can be easily generated with spatial light modulators (SLMs).[16,17] In this regard, Bobkova et al. recently operated both in the phase and amplitude of a multiplexed vortex-generating beam to manage full control of particles' motion on two vortices.[14]

The design of DOEs for vortex beam generation allows engineering multiple configurations, such as the multiplexed vortex phase mask proposed in this work. A vortex beam can be formed from a phase singularity characterized by its topological charge. These vortex beams present an angular momentum composed of an orbital component from the phase and intensity profile and a helical phase caused by their azimuthal phase dependence.[18,19] The aforementioned characteristics make vortex beams potential tools in optical trapping systems. The incorporation of vortex DOEs into an optical tweezers system increases the flexibility and capacity for trapping and manipulating particles.[20–22] Optical vortices transfer angular momentum to trapped particles forcing them to move around the optical axis,[23,24] which is a valuable feature in an optical tweezers system. Furthermore, a spatially multiplexed vortex phase mask allows the generation of simultaneous concentric optical vortices, each constituting a trapping and manipulation system.

Previous works have demonstrated the utility of joint optical vortices as actuators in microfluidic and micromechanical systems.[25,26] Intensity patterns are generally chosen to engineer vortices with the same topological charge,[27,28] a strategy that often constrains their dynamics. The generation of multiplexed vortices through DOEs offers an alternative option in the development of new optical tweezers systems that, through the control of the topological charge, boost the maneuverability at the micro and nanoscales.[29,30]

In this regard, we herein design and implement a new multiplexed vortex DOE in an experimental optical tweezers system. We present the phase mask profile design and numerical summations of the irradiance distribution. We build multiplexed optical vortices with torque-induced orbiting dynamics on confined beads exclusively based on the phase mask, i.e., with phase-only beam modulation. In this regard, this DOE generates spatially multiplexed vortices, and the intrinsic features of the phase mask allow both the multiple trapping of particles and the transfer of angular momentum, which make them orbit around the optical axis independently on each vortex. Experimental results show that multiplexed vortex beams generate stable dynamics in the trapping and particle motion within the concentric rings.

[1]Centro de Tecnologías Físicas, Universitat Politècnica de València, 46022 València, Spain
[2]Laboratorio de Fibra Óptica, Universidad Politécnica de Tulancingo, División de Posgrado, Hidalgo C.P. 43629, México
[3]Departamento de Óptica y Optometría y Ciencias de la Visión, Universitat de València, 46100 Burjassot, Spain
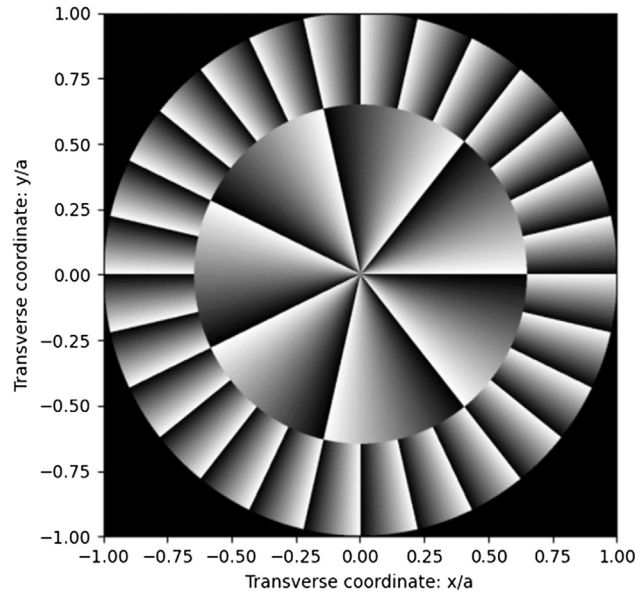[4]Lead contact
*Correspondence: fmmuope1@upvnet.upv.es
https://doi.org/10.1016/j.isci.2023.107987

Figure 1. Phase distributions of an MSPM ($N = 2$, $m_1 = -7$ and $m_2 = 28$)

RESULTS AND DISCUSSION

Multiplexed spiral phase mask design

A spiral phase mask (SPM) is a DOE with a linear phase dependence only on the azimuthal angle. This phase distribution can be achieved by $\Phi(\theta_0) = mod_{2\pi}[m\theta_0]$, where m is the so-called topological charge (an integer number different from zero), and θ_0 is the azimuthal angle taken with respect to the optical axis of the pupil plane. Our strategy for generating multiplexed vortex beams consists on integrating concentric SPMs with independent topological charges. In this regard, a multiplexed SPM (MSPM) is an arrangement of SPMs in concentric annular zones in a single DOE, which phase distribution $\tau(r, \theta_0)$ can be defined by:

$$\tau(r, \theta_0) = \begin{cases} mod_{2\pi}[m_1\theta_0], 0 \leq r < r_1 \\ \dots \\ mod_{2\pi}[m_j\theta_0], r_{j-1} \leq r < r_j , \\ \dots \\ mod_{2\pi}[m_N\theta_0], r_{N-1} \leq r < a \end{cases} \quad \text{(Equation 1)}$$

where r is the radial coordinate, a is the radius of the resulting DOE, N is the total number multiplexed SPMs, and m_j is the topological charge of the j-th SPM limited between radial distances r_{j-1} and r_j, being $r_0 = 0$ and $r_N = a$.

Figure 1 shows the phase distribution of an MSPM ($N = 2$) with topological charges $m_1 = -7$ and $m_2 = 28$ used in this research work. The gray levels represent the phase modulation from 0 to 2π. It is possible to observe the change of sign between the considered topological charges and the number of azimuthal periods corresponding to the value of each topological charge.

Focusing properties with MSPM

The irradiance of the DOE is provided by the transmittance, $t(\zeta, \theta_0) = q(\zeta)\exp[im\theta_0]$, of the diffractive element when it is illuminated by a plane wave of wavelength λ, where $\zeta = (r/a)^2$. Let us now consider an MSPM with a phase distribution given by Equation 1 placed at the exit pupil of a microscope objective. The resulting irradiance within the Fresnel approximation as a function of the axial distance from the pupil plane z is:[31]

$$I(u, v, \theta) = u^2 \left| \sum_{j=1}^{N} \int_{\zeta_{j-1}}^{\zeta_j} \int_0^{2\pi} q(\zeta)\exp(im_j\theta_0)\exp(-i2\pi u\zeta)\exp\left[i4\pi uv\zeta^{1/2}\cos(\theta - \theta_0)\right]d\zeta d\theta_0 \right|^2, \quad \text{(Equation 2)}$$

where $u = a^2/2\lambda z$ is the reduced axial coordinate, $v = r/a$ is the normalized transverse coordinate, and θ is the azimuthal coordinate. By solving the integral for the angular dependence, we find:

$$\int_0^{2\pi} \exp[im_j\theta_0]\exp\left[i4\pi uv\zeta^{1/2}\cos(\theta - \theta_0)\right]d\theta = 2\pi \exp\left[im_j(\theta_0 + \pi/2)\right]J_{m_j}\left(4\pi uv\zeta^{1/2}\right), \quad \text{(Equation 3)}$$

being J_{m_j} the Bessel function of the first kind of order m_j. As a consequence, Equation 2 reduces to
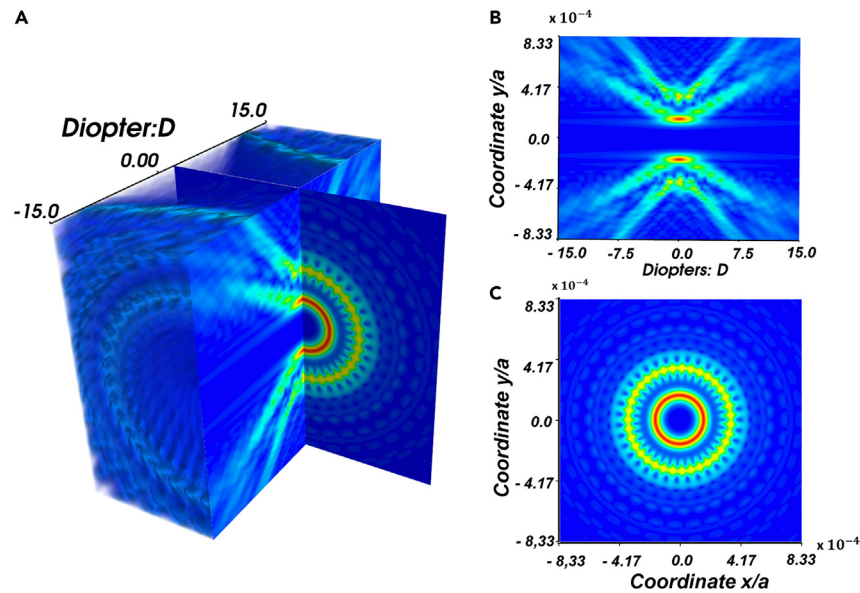
Figure 2. Irradiance computed of an MSPM (N=2) with topological charges $m_1 = -7$ and $m_2 = 28$

(A) Computed irradiance with the MSPM shown in Figure 1.

(B) Longitudinal plane of irradiance on the optical axis.

(C) Transverse plane of irradiance at the focal point.

$$I(u, v) = 4\pi^2 u^2 \left| \sum_{j=1}^{N} \int_{\zeta_{j-1}}^{\zeta_j} q(\zeta) \exp\left(-i2\pi u\zeta\right) J_{m_j}\left(i4\pi uv\zeta^{1/2}\right) d\zeta \right|^2, \qquad \text{(Equation 4)}$$

We have computed the irradiances provided with the MSPM shown in Figure 1 by using Equation 4. The result can be seen in Figure 2, where it is possible to discern two main vortices formed at the focal plane with the outer vortex exhibiting a sinusoidal azimuthal variation. The interference intensity profile stems from the superposition of both vortices as a consequence of the difference in topological charges. The intensity map of the inner vortex is homogeneous at the transverse, focal plane (see Figure 2C), but the outer vortex is constituted of angularly distributed lobes associated to alternating constructive and destructive wave superpositions. The total number of lobes in the outer vortex is 35, which is congruent with the relationship $(m_2 - m_1) = (28 + 7) = 35$ derived elsewhere.[23]

Trapping and manipulation with an MSPM

We present the experimental manipulation of microparticles through the multiplexed vortex beams shown in Figure 2. Our optical setup allows the trapping of several microparticles arranged in two circular rings with nearly independent dynamics. In this regard, Figure 3 shows the steady rotational motion of serial polystyrene beads (diameter ~2 μm) in each vortex. The arrows indicate the direction of particle rotation, consistent with the sign of the topological charges herein used. In particular, since m_1 is negative, the motion of the particles is levorotatory (anti-clockwise, as shown in the depicted planes of Figure 3). The opposite takes place for the outer vortex, where m_2 is positive, making the dynamics dextrorotatory (clockwise in Figure 3).

An individual particle was selected in each concentric vortex for analyzing further the rotational motion in the fluid: the one in the inner vortex is marked with a blue dot, whereas that on the outer vortex with a red dot.

An essential feature of our MSPM-based optical tweezers is the opposite directions between vortices, which are controlled by the topological charges of the phase mask. In this regard, by flipping signs in m_1 and m_2, the two rotational motions of the particles reverse, as observed in Figures 4A–4C. As expected, if the signs are the same for both topological charges, the direction of rotation direction becomes the same for both vortices.

The steady motion of the microparticles is a consequence of the torque exerted by light, which transfers angular momentum to the trapped particles, counteracted by the friction in the fluid environment. For manipulation purposes, we use phase modulation to exert rotational dynamics into confined beads, in contrast to polarization vortex manipulation, which is managed via the azimuthal imaginary Poynting momentum.[32–34] The angular velocity, ω, of the orbiting dynamics depends on the confining vortex. To demonstrate this, we performed a more detailed analysis with a higher magnification objective (100×, NA = 1.3). The results are displayed in Figure 5, where it is observed generally that the angular velocity of the external vortex is lower than that of the internal vortex.
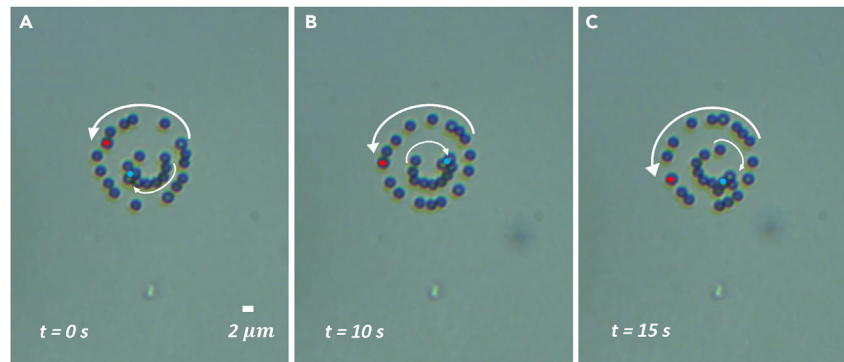
Figure 3. Sequence of images for the dynamic trapping of microparticles around MSPM-based optical tweezers
The inner vortex has a topological charge $m_1 = -7$ and the outer one $m_2 = 28$. See Video S1.
(A) t = 0 sec.
(B) t = 10 sec.
(C) t = 15 sec.

The behavior of the angular velocity as a function of the optical power measured at the focal plane is shown in panels (A) and (B) for different values of m_1 and of the constant topological charge m_2. The angular velocity for the internal vortex increases with the optical power, unlike for the external vortex, which almost remains constant within the experimental error. The angular velocity is higher in the inner vortex as a consequence of the energy concentration due to the smaller diameter (see Figure 5A). The outer vortex, in contrast, enables lower angular velocities due to the spread of the focal irradiance over a larger diameter (see Figure 5B). Both the inner and outer vortices present an onset in the angular velocity increasing trend for an approximate power of 16 mW.

With regards to variations in the topological charge, Figure 5C, it is observed that the rotational motion of the particles in the internal vortex starts at a threshold topological charge right before $m_1 = 4$ and that their angular velocity exhibits a maximum for $m_1 = 7$. The diameter of the internal vortex is smaller than that of the particles for $m_1 \leq 4$, making the vortex approach a point trap, hence only capable of confining a single particle in the vortex center. The particles may present a spin angular momentum due to slight deviations from sphericity, which generate differential friction with the fluid around their surface while moving along the orbiting trajectories. However, we cannot ascertain this within experimental error in our assays. When $m_1 > 7$, the diameter of the internal vortex increases, causing a redistribution of the light power on a larger area at the focal region, which in turn reduces the irradiance and the angular momentum imparted by the photon flux onto the particles. These results are consistent with those of Liang et al.,[28] who studied the behavior of particles within a single vortex. The particles in the outer vortex, in contrast, although they exhibit motion at low values of m_1 (see Figure 5C), their angular velocity increases only slightly with m_1, which is also due to the power distribution on a larger area for this external vortex.

Then, if vortices have sufficiently spaced radii, their superposition is negligible, preventing interactions among particles confined in different vortices. In addition, although the formation of the outer vortex is dependent on the generation of the inner vortex, two free parameters, namely, topological charges m_1 and m_2, control in sufficiently ample ranges of values the following aspects of the vortices for the implementation of orbiting
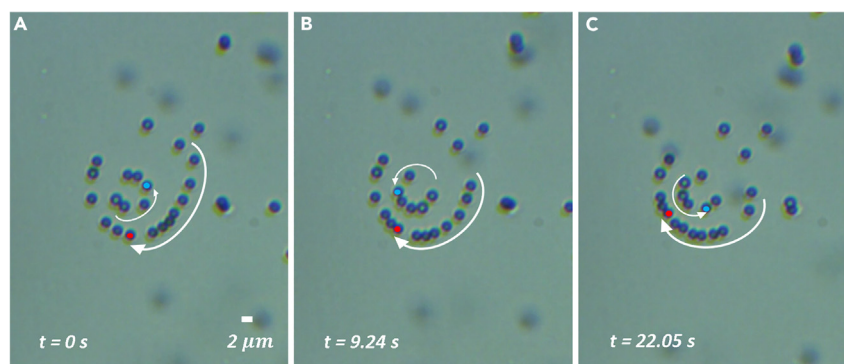

Figure 4. Sequence of images for the dynamic trapping of microparticles around MSPM-based optical tweezers
The inner vortex has a topological charge $m_1 = 7$ and the outer one $m_2 = -28$. See Video S2.
(A) t = 0 sec.
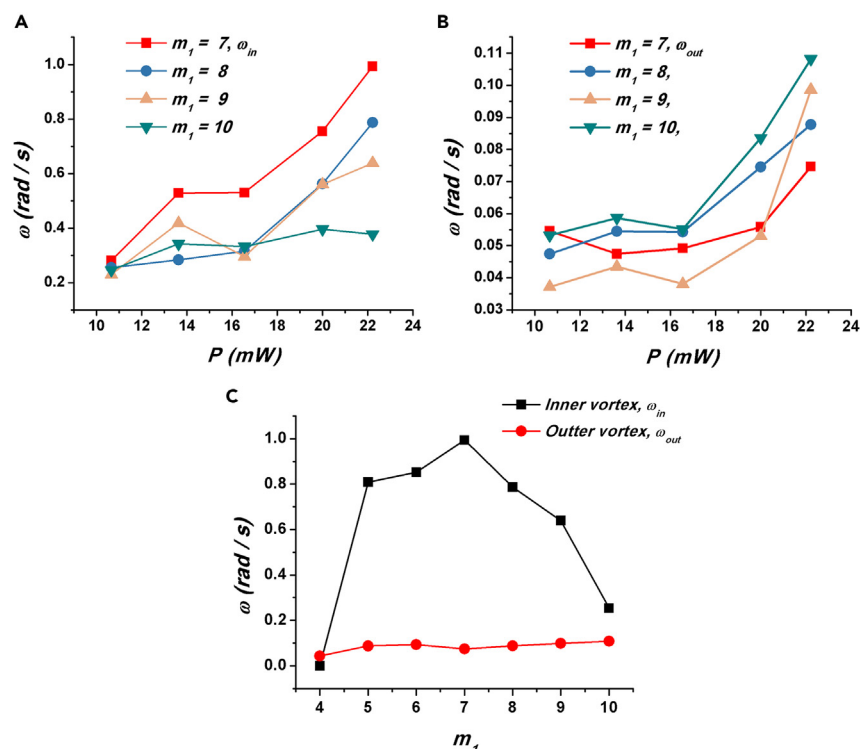(B) t = 9.24 sec.
(C) t = 22.05 sec.

Figure 5. Orbiting dynamics of microparticles in an MSPM with topological charge $m_2 = -38$ and different topological charges of the internal vortex

(A) Modulus of the angular velocity for particles confined in the inner (ω_{in}) vortice vs. optical power at the focal region.

(B) Modulus of the angular velocity for particles confined in the outer (ω_{out}) vortice vs. optical power at the focal region.

(C) Angular velocity for particles confined in the inner and outer vortices vs. topological charge of the internal vortex at a focal power of 22.21 mW.

dynamics: (i) the radii of the inner and outer vortices; (ii) the orbiting direction of trapped particles within each vortex independently; (iii) the relative angular velocity with which particles move in the two vortices. These features enable a nearly independent manipulation from a practical viewpoint.

Conclusions

An MSPM has been designed and implemented on an experimental arrangement of optical tweezers, which allows the trapping and manipulation of particles on each of the vortices formed. This DOE enables the formation on the focal plane of an internal vortex with a topological charge m_1 and an external vortex with a topological charge m_2. The trapped particles move around the circumference of each vortex due to the angular momentum imparted by phase distribution. The direction of rotation is dependent on the sign of each topological charge, with which it is possible to have a different approach in each vortex. The MSPM exhibits a stable trapping capacity of multiple particles in both vortices, regardless of the orbiting direction of spin. With this, the MSPM allow nearly independent rotation control between vortices, opening an alternative to the trapping of microstructures with dynamic manipulation in their rotation. Optical tweezers with holographic techniques are broadening the palette of applications in different areas and, in this regard, the development of MSPMs may contribute to breaking technological limitations in optical dragging, longitudinal optical blinding and both tomographic and super-resolution microscopy. We envision that MSPMs will be implemented in remote control of microrobots, shedding light on how to generate mechanical work at the nanoscale for functioning of microvalves, micromotors and complex nano-gears or for assembling of microstructures.

Limitations of the study

Here, we present the design and implementation of a multiplexed SPM in an experimental configuration of optical tweezers. This DOE allows for the generation of multiple concentric vortex beams with independent topological charges. We experimentally demonstrate the transfer of angular momentum to optically trapped microparticles and analyze the angular velocity of the confined particles. However, this study only shows the angular velocity as a function of optical power in the focal region for different combinations of topological charges. Future work could further investigate the trapping dynamics of multiple particles, as well as study the imaginary Poynting momentum.

STAR★METHODS

Detailed methods are provided in the online version of this paper and include the following:

AUTHOR CONTRIBUTIONS

F.M.M.P., J.R.A.G., and J.A.M. conceived and designed the experiments. F.M.M.P. and V.F. performed the experiments. W.D.F. and J.C.C.P analyzed the data. F.M.M.P. wrote the manuscript.

DECLARATION OF INTERESTS

The authors declare no competing interests.

REFERENCES

1. Simula, T. (2020). Gravitational vortex mass in a superfluid. Phys. Rev. *101*, 063616. https://doi.org/10.1103/PhysRevA.101.063616.

2. Goto, K., Nakajima, k., and Notsu, H. (2021). Twin vortex computer in fluid flow. New J. Phys. *23*, 063051. https://doi.org/10.1088/1367-2630/ac024d.

3. Coullet, P., Gil, L., and Rocca, F. (1989). Optical vortices. Opt. Commun. *73*, 403–408. https://doi.org/10.1016/0030-4018(89)90180-6.

4. Zou, X., Zheng, Q., Wu, D., and Lei, H. (2020). Controllable Cellular Micromotors Based on Optical Tweezers. Adv. Funct. Mater. *30*, 2002081. https://doi.org/10.1002/adfm.202002081.

5. Wang, X., Song, Y., Zhang, Q., Pang, F., Li, Y., and Cao, B. (2018). Interconnecting data based on vortex beams by adjusting the ellipticity of a ring-core fiber. Appl. Opt. *57*, 7492–7500. https://doi.org/10.1364/AO.57.007492.

6. Fang, X., Ren, H., and Gu, M. (2020). Orbital angular momentum holography for high-security encryption. Nat. Photonics *14*, 102–108. https://doi.org/10.1038/s41566-019-0560-x.

7. Gong, L., Zhao, Q., Zhang, H., Hu, X.-Y., Huang, K., Yang, J.-M., and Li, Y.-M. (2019). Optical orbital-angular-momentum-multiplexed data transmission under high scattering. Light Sci. Appl. *8*, 27. https://doi.org/10.1038/s41377-019-0140-3.

8. Gbur, G., and Visser, T.D. (2006). Phase singularities and coherence vortices in linear optical systems. Opt Commun. *259*, 428–435. https://doi.org/10.1016/j.optcom.2005.08.074.

9. Furlan, W.D., Giménez, F., Calatayud, A., and Monsoriu, J.A. (2009). Devils vortex-lenses. Opt Express *17*, 21891–21896. https://doi.org/10.1364/OE.17.021891.

10. Paterson, L., MacDonald, M.P., Arlt, J., Sibbett, W., Bryant, P.E., and Dholakia, K. (2001). Controlled rotation of optically trapped microscopic particles. Science *292*, 912–914. https://doi.org/10.1126/science.1058591.

11. Liang, Y., Yan, S., Wang, Z., Li, R., Cai, Y., He, M., Yao, B., and Lei, M. (2020). Simultaneous optical trapping and imaging in the axial plane: a review of current progress. Rep. Prog. Phys. *83*, 032401. https://doi.org/10.1088/1361-6633/ab7175.

12. Gahagan, K.T., and Swartzlander, G.A., Jr. (1996). Optical vortex trapping of particles. Opt. Lett. *21*, 827–829. https://doi.org/10.1364/OL.21.000827.

13. Lee, W.M., Yuan, X.-C., and Cheong, W.C. (2004). Optical vortex beam shaping by use of highly efficient irregular spiral phase plates for optical micromanipulation. Opt. Lett. *29*, 1796–1798. https://doi.org/10.1364/OL.29.001796.

14. Bobkova, V., Stegemann, J., Droop, R., Otte, E., and Denz, C. (2021). Optical grinder: sorting of trapped particles by orbital angular momentum. Opt Express *29*, 12967–12975. https://doi.org/10.1364/OE.419876.

15. Tao, S.H., Yuan, X.-C., Lin, J., and Burge, R.E. (2006). Sequence of focused optical vortices generated by a spiral fractal zone plate. Appl. Phys. Lett. *89*, 031105. https://doi.org/10.1063/1.2226995.

16. Muoz-Pérez, F.M., Ferrando, V., Furlan, W.D., Monsoriu, J.A., and Ricardo Arias-Gonzalez, J. (2022). Optical multi-trapping by Kinoform m-Bonacci lenses. Opt Express *30*, 34378–34384. https://doi.org/10.1364/OE.465672.

17. Calatayud, A., Ferrando, V., Remón, L., Furlan, W.D., and Monsoriu, J.A. (2013). Twin axial vortices generated by Fibonacci lenses. Opt Express *21*, 10234–10239. https://doi.org/10.1364/OE.21.01023.

18. Schmitz, C.H.J., Uhrig, K., Spatz, J.P., and Curtis, J.E. (2006). Tuning the orbital angular momentum in optical vortex beams. Opt Express *14*, 6604–6612. https://doi.org/10.1364/OE.14.006604.

19. Roux, F.S. (2004). Distribution of angular momentum and vortex morphology in optical beams. Opt Commun. *242*, 45–55. https://doi.org/10.1016/j.optcom.2004.08.006.

20. Gecevičius, M., Drevinskasa, R., Beresna, M., and Kazansky, P.G. (2014). Single beam optical vortex tweezers with tunable orbital angular momentum. Appl. Phys. Lett. *104*, 231110. https://doi.org/10.1063/1.4882418.

21. Padgett, M., and Bowman, R. (2011). Tweezers with a twist. Nat. Photonics *5*, 343–348. https://doi.org/10.1038/nphoton.2011.81.

22. Liang, Y., Lei, M., Yan, S., Li, M., Cai, Y., Wang, Z., Yu, X., and Yao, B. (2018). Rotating of low-refractive-index microparticles with a quasi-perfect optical vortex. Appl. Opt. *57*, 79–84. https://doi.org/10.1364/AO.57.000079.

23. Machado, F., Zagrajek, P., Ferrando, V., Monsoriu, J.A., and Furlan, W.D. (2019). Multiplexing THz Vortex Beams with a Single Diffractive 3-D Printed Lens. IEEE Trans. Terahertz Sci. Technol. *9*, 63–66. https://doi.org/10.1109/TTHZ.2018.2883831.

24. Morgan, K.S., Miller, J.K., Cochenour, B.M., Li, W., Li, Y., Watkins, R.J., and Johnson, E.G. (2016). Free space propagation of concentric vortices through underwater turbid environments. IOP *J. Opt*. J. Opt. *1810*, 104004. https://doi.org/10.1088/2040-8978/18/10/104004.

25. Bishop, A.I., Nieminen, T.A., Heckenberg, N.R., and Rubinsztein-Dunlop, H. (2003). Optical application and measurement of torque on microparticles of isotropic nonabsorbing material. Phys. Rev. *68*, 033802. https://doi.org/10.1103/PhysRevA.68.033802.

26. Ladavac, K., and Grier, D. (2004). Microoptomechanical pumps assembled and driven by holographic optical vortex arrays. Opt Express *12*, 1144–1149. https://doi.org/10.1364/opex.12.001144.

27. Li, X., Zhou, Y., Cai, Y., Zhang, Y., Yan, S., Li, M., Li, R., and Yao, B. (2021). Generation of Hybrid Optical Trap Array by Holographic Optical Tweezers. Front. Physiol. *9*, 591747. https://doi.org/10.3389/fphy.2021.591747.

28. Tian, Y., Wang, L., Duan, G., and Yu, L. (2021). Multi-trap optical tweezers based on composite vortex beams. Opt Commun. *485*, 126712. https://doi.org/10.1016/j.optcom.2020.126712.

29. Pu, J., and Jones, P.H. (2015). Devil's lens optical tweezers. Opt Express *237*, 8190–8199. https://doi.org/10.1364/OE.23.008190.

30. Cheng, S., Zhang, X., Ma, W., and Tao, S. (2016). Fractal zone plate beam based optical tweezers. Sci. Rep. *6*, 34492. https://doi.org/10.1038/srep34492.

31. Goodman, J.W. (2016). Introduction to Fourier Optics, 3rd edition (Springer).

32. Nieto-Vesperinas, M., and Xu, X. (2022). The complex Maxwell stress tensor theorem: The imaginary stress tensor and the reactive strength of orbital momentum. A novel scenery underlying electromagnetic optical forces. Light Sci. Appl. *11*, 297. https://doi.org/10.1038/s41377-022-00979-2.

33. Xu, X., and Nieto-Vesperinas, M. (2019). Azimuthal Imaginary Poynting Momentum Density. Phys. Rev. Lett. *123*, 233902. https://doi.org/10.1103/PhysRevLett.123.233902.

34. Zhou, Y., Xu, X., Zhang, Y., Li, M., Yan, S., Nieto-Vesperinas, M., Li, B., Qiu, C.W., and Yao, B. (2022). Observation of high-order imaginary Poynting momentum optomechanics in structured light. Proc. Natl. Acad. Sci. USA *119*, 1–9. https://doi.org/10.1073/pnas.2209721119.

STAR★METHODS

KEY RESOURCES TABLE

REAGENT or RESOURCE	SOURCE	IDENTIFIER
Software and algorithms		
Visual Studio Code	Visual Studio Code	https://code.visualstudio.com/
Python	Python	https://www.python.org/
Other		
Polystyrene Particles	Spherotech	PP-20-10

RESOURCE AVAILABILITY

Lead contact

Further information and requests should be directed to and will be fulfilled by the lead contact, Francisco M. Muñoz-Pérez (fmmuope1@upvnet.upv.es).

Materials availability

This study did not generate new unique materials

Data and code availability

- The most relevant data have been reported in the document and in the supplemental information.
- This paper does not report original code.
- Any additional information required to reanalyze the data reported in this paper is available from the lead contact upon request (fmmuope1@upvnet.upv.es).
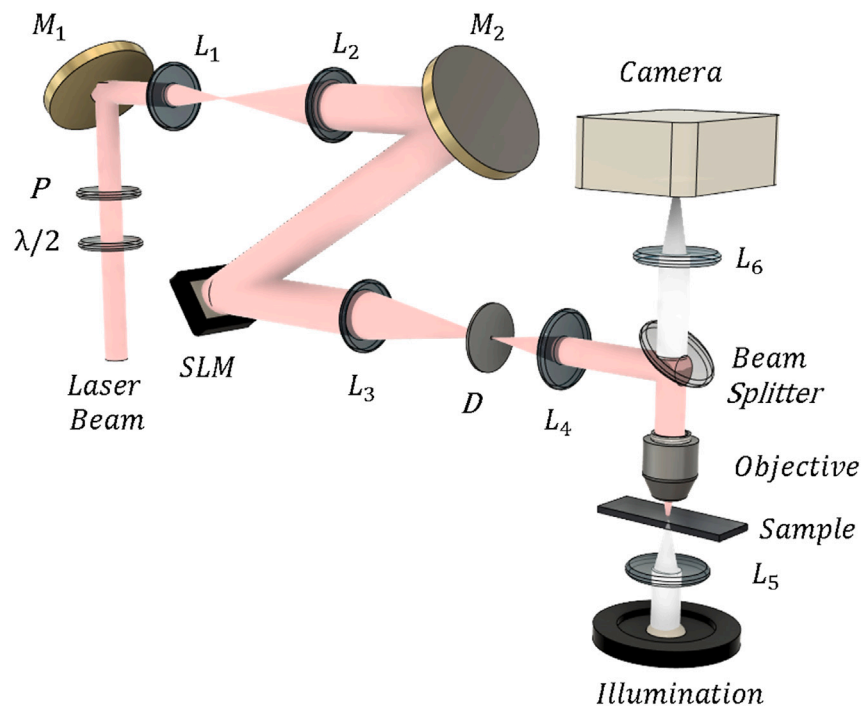
EXPERIMENTAL MODEL AND STUDY PARTICIPANT DETAILS

Our study does not use experimental models typical in the life sciences.

METHODS DETAILS

Material

Multiplexed Spiral Phase Mask (MSPM) for confined, rotational dynamics were set up in an optical tweezers design,[14] as represented in below figure.

Experimental optical tweezers setup to confine particles by using MSPMs
The beam is spatially filtered by a diaphragm (*D*) placed at the focus of L_3, which lets only the first diffraction order pass. The SLM is tilted slightly to compensate for the added linear phase carrier, thus allowing the first-order diffraction to align with the optical axis of the diaphragm. The MSPM image is then passed through either a 40× objective or a high-numerical aperture oil-immersion objective (Olympus UPLFLN 100×, NA = 1.3) used for rotational dynamics analysis, positioned at the focal plane L_4. The sample is illuminated with an LED light source (Thorlabs, Mounted High-Power, 1300 mA, Mod. MCWHL7) and the light collimated and focused on the sample through lens L_5 (f_5 = 30 mm). A beam splitter (BS) allows the transmission of the visible light from the sample through the rear focal plane of the objective. The BS prevents reflections of infrared light from being transmitted to the imaging system. The resulting image is focused with lens L_6 (f_6 = 50 mm). A CMOS camera (Edmund Optics, Mod. EO-10012C) is used for imaging purposes of the particles at the confining plane. +.

In short, a continuous wave laser beam (λ = 1064 nm, Laser Quantum, Mod. Opus 1064) is incident on a half-wave plate ($\lambda/2$) followed by a linear polarizer (*P*), which lets the direction of the linear polarization of the beam to be set. The laser beam is guided by mirrors (*M1* and *M2*) onto a ×3 beam expander, as formed by lenses *L1* and *L2* (focal length f_1 = 50 mm and f_2 = 150 mm). The MSPM is projected onto a spatial light modulator (SLM) display (Holoeye PLUTO-2.1-NIR-149, phase type, pixel size 8 μm and resolution 1920 x 1080 pixels). A 1D blazed grating is added to each MSPM, which purpose is to act as a linear phase carrier. It allows the diffracted light to be conducted towards the first order of diffraction, thus preventing noise caused by specular reflection from higher diffraction orders. The SLM is configured for a phase of 2.1π at a wavelength λ = 1064 nm. The modulated MSPM beam in the SLM is reduced by a 4f system consisting of L_3 (f_3 = 150 mm) and L_4 (focal length f_4 = 150 mm).

Multiplexed spiral phase mask generation

The multiplexed spiral phase mask has only a linear phase dependence on the azimuthal angle, and generated using Equation 1. Our strategy for generating multiplexed vortex beams, consists on integrating concentric SPMs with independent topological charges. In this regard, a multiplexed SPM (MSPM) is an arrangement of SPMs in concentric annular zones in a single DOE.

QUANTIFICATION AND STATISTICAL ANALYSIS

There is no statistical analysis in this paper.

ADDITIONAL RESOURCES

We have no relevant resources.